3-27-2017

Photochemical Properties and Structure-Activity Relationships of Ru^{II} Complexes with Pyridylbenzazole Ligands as Promising Anticancer Agents

Dmytro Havrylyuk
University of Kentucky, dyha223@uky.edu

David K. Heidary
University of Kentucky, david.heidary@uky.edu

Leona Nease
University of Kentucky

Sean Parkin
University of Kentucky, s.parkin@uky.edu

Edith C. Glazer
University of Kentucky, ec.glazer@uky.edu

Photochemical Properties and Structure-Activity Relationships of Ru^{II} Complexes with Pyridylbenzazole Ligands as Promising Anticancer Agents

Notes/Citation Information
Published in *European Journal of Inorganic Chemistry*, v. 2017, issue 12, p. 1687-1694.

Digital Object Identifier (DOI)
https://doi.org/10.1002/ejic.201601450

Published in final edited form as:

Eur J Inorg Chem. 2017 March 27; 2017(12): 1687–1694. doi:10.1002/ejic.201601450.

Photochemical Properties and Structure–Activity Relationships of Ru^{II} Complexes with Pyridylbenzazole Ligands as Promising Anticancer Agents

Dmytro Havrylyuk, **David K. Heidary**, **Leona Nease**, **Sean Parkin**, and **Edith C. Glazer**[a]

[a]Department of Chemistry, University of Kentucky, 505 Rose Street, Lexington, Kentucky 40506, United States

Abstract

Ruthenium complexes capable of light-triggered cytotoxicity are appealing potential prodrugs for photodynamic therapy (PDT) and photoactivated chemotherapy (PACT). Two groups of Ru(II) polypyridyl complexes with 2-(2-pyridyl)-benzazole ligands were synthesized and investigated for their photochemical properties and anticancer activity to compare strained and unstrained systems that are likely to have different biological mechanisms of action. The structure-activity relationship was focused on the benzazole core bioisosterism and replacement of coligands in Ru(II) complexes. Strained compounds rapidly ejected the 2-(2-pyridyl)-benzazole ligand after light irradiation, and possessed strong toxicity in the HL-60 cell line both under dark and light conditions. In contrast, unstrained Ru(II) complexes were non-toxic in the absence of light, induced cytotoxicity at nanomolar concentrations after light irradiation, and are capable of light-induced DNA damage. The 90−220-fold difference in light and dark IC_{50} values provides a large potential therapeutic window to allow for selective targeting of cells by exposure to light.

Keywords

synthesis; photochemistry; cytotoxicity; DNA damage; ruthenium

Introduction

Cancer is currently the second leading cause of death in the United States, following heart disease. More than 1.7 million people are estimated to be diagnosed with cancer in 2016.[1] With global cancer morbidity rising, the development of new cancer treatments is crucial. Chemotherapy is used in most treatment regimens for cancer. Since its discovery in the late 1960s, cisplatin and derivatives thereof have achieved great success, and nearly 50% of patients being treated for cancer are given a platinum based drug.[2] Widespread treatment with cisplatin, however, revealed major clinical problems associated with its use. Cisplatin has dose-limiting side effects, such as nephrotoxicity, neurotoxicity, ototoxicity, and myelosuppression.[3] Due to these severe side effects, cisplatin has to be administered at

Correspondence to: Edith C. Glazer.

Supporting information for this article is given via a link at the end of the document.

concentrations that might not be lethal to tumor cells, thereby facilitating development of drug resistance. These limitations have driven the investigations of other (non-platinum) transition metal compounds.

In recent years, ruthenium-based complexes have emerged as promising antitumor and antimetastatic agents with potential uses in platinum-resistant tumors.[4] Ruthenium compounds are well suited for medical applications due to a combination of chemical and biological properties: they can form multiple geometries with facile ligand exchange, they can be activated by environmental features or external triggers, and they are capable of mimicking iron binding for transportation.[5] The different oxidation states can be exploited to design prodrugs, where the inactive 3+ ruthenium complexes can be reduced to 2+, creating an active species and a biological effect. The reducing environment of tumors has been associated with the selective activity of ruthenium-based drugs NAMI-A, KP1019, and KP1339, which have been investigated in clinical trials.[6] An alternative prodrug strategy is to use light to transform inert complexes into cytotoxic agents.[7] We have demonstrated that this can be accomplished with strained Ru(II) polypyridyl complexes with distorted octahedral geometry, which photo-decompose via ligand dissociation.[8] The resulting ligand-deficient Ru(II) center can covalently modify DNA or other biomolecules, and induce cytotoxicity.[9]

The application of light-mediated ruthenium complexes can be divided into two categories: photodynamic therapy (PDT) and photoactivated chemotherapy (PACT).[10] PDT relies mainly on the generation of the toxic reactive oxygen species (ROS) such as singlet oxygen ($^1O_2$). In contrast, PACT exploits different mechanisms to induce cell death, such as ligand ejection to create metal centers able to form DNA adducts, or photocaging approaches. In this article, we present the investigation of strained and unstrained ruthenium (II) complexes with 2-(2-pyridyl)-benzazole ligands as promising antitumor agents with possible application in both PDT and PACT.

The benzazole moiety was chosen as it combines features including extended conjugation for modulation of the absorption profile, and the potential for intrinsic steric clash within a coordination complex, similar to quinoline-containing ligands.[8b] It also facilitated a systematic investigation as it provided a single point for chemical variation, with a heteroatom (N, O, S) at the 1-position with a nitrogen at the 3-position, or a carbon at the analogous position in indole (Scheme 1). Moreover, benzazole-containing systems exhibit a variety of biological activities and applications. Recently, organometallic systems containing this ligand type have been explored, including half-sandwich ruthenium(II) arene compounds with pyridyl-benzimidazole ligands studied for their DNA binding ability,[11] cyclin-dependent kinase (CDK1) inhibitory effects,[11b] and inhibition of protein tyrosine phosphatase (PTP-1B).[12] The previous investigations of ruthenium complexes with aryl-benzimidazole ligands showed cytotoxic effect at μM concentrations.[11b, 13]

In this report, we have discovered that coordination of non-cytotoxic 2-(2-pyridyl)-benzazole ligands with a $Ru(dmphen)_2$ (dmphen = 2,9-dimethyl-1,10-phenanthroline) scaffold, forming strained Ru(II) complexes, promoted significant cytotoxic potential of compounds with single μM IC_{50} values both in dark and light conditions. In contrast, the

complexes with 2,2′-bipyridine (bpy) ligands were not active in the absence of light. However, these compounds were effective in killing cells when irradiated, producing nM IC_{50} values. DNA damage analysis and evaluation of singlet oxygen production confirmed that unstrained compounds generate toxic ROS. However, the disparity in the effective concentration and trends for cytotoxicity (IC_{50}< 1 μM) and singlet oxygen generation (> 10 μM) suggests that these compounds act through some additional, currently unknown, mechanism(s) of action.

Results and Discussion

Synthesis and Characterization

To explore structure-activity relationships (SAR), a small family of heteroleptic Ru(II) complexes (**5–12**) were synthesized that contained one 2-(2-pyridyl)benzazole type ligand and two strain-inducing dmphen ligands or two bpy ligands as shown in Scheme 1. Four heterocyclic bioisosteres were studied: 2-(2-pyridyl)indole (pi) **1**, 2-(2-pyridyl)benzimidazole (pbi) **2**, 2-(2-pyridyl)benzoxazole (pbo) **3** and 2-(2-pyridyl)benzothiazole (pbt) **4**. These systems were chosen in order to investigate the impact of replacement of one pyridyl-type ligand with a benzazole on the cytotoxicity and photochemical properties of the Ru(II) complexes.

The Ru(II) complexes were synthesized from a racemic mixture of the Δ and Λ enantiomers of $Ru(dmphen)_2Cl_2$ or $Ru(bpy)_2Cl_2$ and thus form a mixture of enantiomers upon coordination of the pyridyl-benzazole ligands. All complexes were exhaustively purified to ensure no contamination of either free ligands or coordinatively unsaturated Ru(II) centers. As the pyridyl-indole is deprotonated, the complexes carry a +1 charge; all other complexes are +2 charged. The complexes were characterized by ^{1}H NMR spectroscopy, ESI-MS, X-ray and UV (see Figure S6–10, S18–27 in the Supporting Information). The strained complexes **5**–**8** were synthesized and characterized for the first time; the unstrained complexes **9**–**12** have been described previously.[14] In contrast to the described ^{1}H NMR spectra (300 MHz, CD_3CN) for **11** and **12**,[14b] we observed that some resonances for H4 and H5 of bpy coligands were resolved as doublet of doublets of doublets (ddd).[15]

X-ray Crystallography

The structures of complexes **6**–**8** were determined by X-ray crystallography and are shown in Figure 1. Selected bond lengths and angles are listed in Table 1.

As expected, complexes **6**–**8** exhibited distorted octahedral geometries. Incorporation of two dmphen ligands resulted in the Ru−N bond lengthening to 2.108 Å (average value for **6**), 2.103 Å (average value for **7**), and 2.105 Å (average value for **8**), in comparison with 2.040–2.059 Å for the corresponding complexes with bpy coligands.[14b, 16] The bond length to the pyridine ring (Ru-N5) is shorter in the pbo and pbt ligands than the bond to the benzazole ring, while the Ru-N6 bond to the benzimidazole is shorter than to the pyridine ring in **6** (Table 1). In contrast to complexes containing the 2,2′-biquinoline ligand,[8b] the two ring systems in the benzazole-containing ligands are essentially co-planar, and do not contribute significantly to the distortion in the complexes.

The bond angles between dmphen ligands are nonequivalent, with the largest distortion from the ideal 90° and 180° for complex **8**. These deviations are larger than for unstrained compound **11** (Figure S5).[14b] Both the dmphen ligands (L1 and L2, Figure 1, Table 1) for each compound **6**–**8** are considerably bent from the normal plane, with deviations of 19.5–22.7°. While the bend angle for L1 is the same for all complexes, the bends of L2 are not equivalent for **6**–**8**, creating variations in strain in the molecules that could cause the difference in photoejection kinetics (Table 2).

Photochemistry

The photochemical reaction of strained Ru(II) complexes **5**–**9** were monitored by absorption spectroscopy, and exhibited selective photoejection of one ligand when irradiated with >450 nm light, as shown in Figure 2A and Figures S6–10. The presence of an isobestic point indicated the direct conversion to a single product (Figure 2A). The half-life ($t_{1/2}$) of ligand ejection in water for **6**–**8** is 40–140× faster than for **5**.

Complex **8** exhibited the fastest ejection, and also the largest bend of dmphen ligand (L2, Table 1), indicating a correlation between the strain in the complex and the photochemical properties. The half-life was also found to be sensitive to the environment, as compound **6** demonstrated a 9-fold slower ligand ejection in Opti-MEM, the media used in tissue culture experiments, than in water (Table 2).

The selective ejection of the 2-(2-pyridyl)benzazole ligands after irradiation of **6**–**8** in water was confirmed by HPLC by comparison with starting complex and ligands (Figure 2E; the same light dose was used as in the cell experiments). Most unstrained Ru(II) complexes with bpy coligands (**10**–**12**) did not eject after 4 h irradiation, but complex **9** gave a $t_{1/2}$ of 66 min (Table 2).

Cytotoxicity, SAR and DNA Damage

An SAR study was performed for 2-(2-pyridyl)benzazole ligands based on benzazole core bioisosterism and the corresponding Ru(II) complexes with dmphen or bpy coligands. None of the free ligands exhibited activity against a leukemic cell line (HL60 human promyelocytic leukemia) up to 100 μM concentrations (Figure 3, Table 3). Compounds **5**–**8** were 20–300-fold more potent against HL60 cell line than parent ligands, with IC_{50} values ranging from 0.34–4.55 μM. Unexpectedly, the photoreactive compounds **6**–**8** exhibited the same range of activity under dark and light conditions. However, the strained Ru(II) complexes exhibited a steeper dose response when light activated, and caused essentially complete cell death in lower concentrations (Figure 3A).

For the photoejecting systems, the largest Phototoxicity Index (PI) value was found for complex **5**, which produced a 10-fold enhanced activity upon irradiation, with a 34 nM IC_{50} value (Table 3). The highest PI values were found for **10**–**12**, which contain the $Ru(bpy)_2$ scaffold. After irradiation, compounds **9**, **10**, and **12** produced submicromolar IC_{50} values, with 7–220-fold differences in the light and dark, and demonstrated 3–17-fold greater potencies than cisplatin. The 88-fold (**12**, Figure S13) and 224-fold (**10**, Figure 3B)

difference in light and dark IC_{50} values provides a large potential therapeutic window to allow for selective targeting of cells by exposure to light.

The SAR study revealed the following: (1) coordination of 2-(2-pyridyl)benzazole ligands with the Ru(II) scaffolds is crucial for potency; (2) the cytotoxic effect is sensitive to the coligands (dmphen vs bpy) – replacement of dmphen with bpy decreased the potency in the dark, but promoted the nM activity after light irradiation (compounds **9**, **10**, **12**) and provided a large potential therapeutic window (88 for **12** and >220 for **10**); (3) the nature of a benzazole core had an influence on the antitumor activity, with complexes **5** and **9** exhibiting 5–35-fold greater potency under dark conditions in comparison to other compounds from strained and unstrained groups, respectively (Table 3, Figure 4). It should be noted that complexes 5 and 9 carry a +1 charge, while all other compounds were +2.

The effect of the compounds **8** and **12** on cell cycle was analyzed at the IC_{50} of the compounds over several time points (Figures S15,16). At the 24 h time point, the sub-G1 phase had increased to 45% of the population for **8** and 27% for **12** when the compounds had been irradiated. No significant increase in the population of apoptotic cells and the G1, S or G2/M populations occurred for **8** and **12** in the dark. Thus, neither compound induced cell cycle arrest under dark conditions or upon irradiation.

In an attempt to determine a potential mechanism of action, DNA damage was assessed by agarose gel electrophoresis. Supercoiled pUC19 plasmid was incubated with each complex in dose response and kept in the dark or exposed to 470 nm light for one hour (Figure 5). The irradiated samples revealed significant differences in damage profiles. The strained photoactive Ru(II) complexes **6** and **8** exhibited a combination of DNA photocleavage and DNA photobinding (Figure 5A, B). Covalent adducts were visualized by the reduced mobility on the agarose gel with increasing concentration of Ru(II) complex, as well as loss of EtBr signal. Unstrained complex **12** induced single-strand breaks in the DNA when irradiated with light, likely due to the photogeneration of $^1O_2$. This was visualized by the conversion from supercoiled DNA to relaxed circle (Figure 5D). Unexpectedly, unstrained **10** produced fewer single-strand breaks than **12** based on the small ratio between relaxed circle and supercoiled DNA (Figure 5C). Precipitation of the DNA with the complexes **5**, **8**, and **9** was observed at concentrations above 125 μM.

Despite the difference in their ability to inflict DNA damage, both the unstrained compounds **10** and **12** induced submicromolar cytotoxicity after light irradiation and exhibited large PI values. In an attempt to confirm or disprove the involvement of light-activated generation of $^1O_2$ in the biological mechanism of action, dose responses of compounds were performed with Singlet Oxygen Sensor Green reagent with light irradiation (Figure 5E; Figure S15). As anticipated, photogeneration of $^1O_2$ was observed for both unstrained complexes **10** and **12**, in contrast to corresponding strained compounds **6** and **8**. Consistent with the DNA damage gels, compound **12** exhibited greater potency for $^1O_2$ generation; however, there is a large discrepancy between the concentrations needed to produce $^1O_2$ or induce strand breaks in the DNA compared to cytotoxicity IC_{50} values. This suggests that $^1O_2$ alone cannot be responsible for the potent effects in cells.[17] Moreover, the pyridyl-indole based complexes

(**5** and **9**) possessed the highest cytotoxicity and did not generate $^1O_2$ upon irradiation (Figure S15).

CONCLUSIONS

Eight heteroleptic Ru(II) complexes were synthesized in order to explore structure−activity relationships. The complexes contained one 2-(2-pyridyl)benzazole type ligand combined with either two dmphen ligands to make intrinsically strained complexes, or two 2,2′-bipyridine ligands to form unstrained complexes. While the free benzazole type ligands **1**–**4** were not toxic in the investigated concentration range, the Ru(II) complexes exhibited marked cytotoxicity. The most potent compounds, **5** and **9**, contained the 2-(2-pyridyl)indole ligand, and were highly effective in killing leukemic cells when irradiated, with IC_{50} values less than 0.04 and 0.2 μM. However, the observed high toxicity in the dark could be a limitation for their potential application as PDT agents.

In contrast, large therapeutic windows were found for complexes **12** and **10** (with 88- and 224-fold differences in light and dark IC_{50} values), which demonstrated 3–15-fold greater potency than cisplatin. The unstrained compounds are capable of generating singlet oxygen, but the significant disparity in the effective concentration for cytotoxicity, $^1O_2$ production, and DNA cleavage suggests that some other, currently unknown, mechanisms of action could be involved for anticancer activity. This may involve different species of ROS.

Considering the promising dark-cytotoxicity of strained complexes and light-induced antitumor potential of unstrained compounds, we are currently modifying these complexes, aiming to generate more potent anticancer agents with possible application in both standard chemotherapy and photodynamic therapy.

EXPERIMENTAL SECTION

Materials and Methods

The starting 2-(2-pyridyl)benzazole ligands were obtained from commercial sources (**2**,**3**) or were synthesized according to the methods described previously (**1**,**4**).[18] Complexes **10–12** were synthesized using previously established procedures.[14]

All ^{1}H NMR spectra were obtained on a Varian Mercury spectrometer (400 MHz) with chemical shifts reported relative to the residual solvent peak of acetonitrile at δ 1.94. Electrospray ionization mass spectra were obtained on a Varian 1200L mass spectrometer. Absorption spectra were obtained on an Agilent Cary 60 spectrophotometer or a BMG Labtech FLUOstar Omega microplate reader. Photoejection, DNA damage, and singlet oxygen generation experiments were performed using a 470 nm LED array from Elixa, and a Loctite Indigo LED array (for cell cytotoxicity studies and HPLC photoejection analysis). All synthesized compounds were isolated in >95% purity, as determined by analytical HPLC. For HPLC analysis, the ruthenium complexes were injected on an Agilent 1100 series HPLC equipped with a model G1311 quaternary pump, G1315B UV diode array detector, and ChemStation software version B.01.03. Chromatographic conditions were optimized on a Column Technologies Inc. C18, 120 Å (250 mm × 4.6 mm inner diameter, 5

μM) fitted with a Phenomenex C18 (4 mm × 3 mm) guard column. Injection volumes of 15 μL of 100 μM solutions of the complex were used. The detection wavelength was 280 nm. Mobile phases were: mobile phase A, 0.1% formic acid in dH_2O; mobile phase B, 0.1% formic acid in HPLC grade acetonitrile. The mobile phase flow rate was 1.0 mL/min. The following mobile phase gradient was used: 98−95% A (containing 2− 5% B) from 0 to 5 min; 95−70% A (5−30% B) from 5 to 15 min; 70−40% A (30−60% B) from 15 to 20 min; 40−5% A (60−95% B) from 20 to 30 min; 5−98% A (95−2% B) from 30 to 35 min; reequilibration at 98% A (2% B) from 35 to 40 min.

General procedure for synthesis of $Ru(dmphen)_2L$ complexes with 2-(2-pyridyl)benzazole ligands

$Ru(dmphen)_2Cl_2$ (1 eq) and 2-(2-pyridyl)benzazole (1.1 eq) were added to 4 mL of ethylene glycol in a 15 mL pressure tube. The mixture was heated at 100–120 °C for 2 h while protected from light. The dark brown (**5**) or orange solution (**6**–**8**) was allowed to cool to room temperature and poured into 50 mL of dH_2O. Addition of a saturated aq. KPF_6 solution (ca. 1 mL) produced a brown or red-orange precipitate that was collected by vacuum filtration. The purification of the solid was carried out by flash chromatography (silica gel, loaded in 0.1% KNO_3, 5%H_2O in MeCN). A gradient was run, and the pure complex eluted at 0.2% KNO_3, 5–10% H_2O in MeCN. The product fractions were concentrated under reduced pressure, and a saturated aq solution of KPF_6 was added, followed by extraction of the complex into CH_2Cl_2. The solvent was removed under reduced pressure to give a solid.

5 R_f=0.63 (0.1% KNO_3, 5%H_2O in MeCN); ^{1}H NMR (CD_3CN): δ 8.59 (d, *J* = 8.2 Hz, 1H), 8.52 (d, *J* = 8.3 Hz, 1H), 8.21 (d, *J* = 8.3 Hz, 1H), 816 (d, *J* = 8.7 Hz, 1H), 8.02–8.06 (m, 3H), 7.81 (d, *J* = 8.7 Hz, 1H), 7.74 (d, *J* = 8.3 Hz, 1H), 7.70 (d, *J* = 8.0 Hz, 1H), 7.64 (d, *J* = 8.3 Hz, 1H), 7.44 (t, *J* = 7.8 Hz, 1H), 7.32 (d, *J* = 8.3 Hz, 1H), 7.28 (d, *J* = 8.3 Hz, 1H), 7.20 (d, *J* = 8.0 Hz, 1H), 6.93 (s, 1H), 6.57 (d, *J* = 5.6 Hz, 1H), 6.43–6.47 (m, 2H), 6.13 (d, *J* = 7.5 Hz, 1H), 4.47 (d, *J* = 8.5 Hz, 1H), 2.02 (s, 3H), 1.98 (s, 3H), 1.85 (s, 3H), 1.82 (s, 3H); purity by HPLC = 97 %; ESI MS calcd for $C_{41}H_{33}N_6Ru$ $[M]^+$ 711.18, found 711.3 $[M]^+$; UV/Vis (CH_3CN): λ^{max} (ε) 490 nm (8400 $mol^{-1}dm^3cm^{-1}$).

6 R_f=0.38 (0.1% KNO_3, 5%H_2O in MeCN); ^{1}H NMR (CD_3CN): δ 8.69 (d, *J* = 8.3 Hz, 1H), 8.62 (d, *J* = 8.3 Hz, 1H), 8.30 (d, *J* = 8.3 Hz, 1H), 8.23 (d, *J* = 8.8 Hz, 1H), 8.09–8.15 (m, 3H), 8.00 (d, *J* = 7.9 Hz, 1H), 7.82–7.88 (m, 3H), 7.72 (d, *J* = 8.3 Hz, 1H), 7.36–7.43 (m, 3H), 7.15 (t, *J* = 7.4 Hz, 1H), 6.93–7.00 (m, 3H), 6.72 (ddd, *J* = 8.8, 7.3, 0.9 Hz, 1H), 4.91 (d, *J* = 8.5 Hz, 1H), 1.98 (s, 3H), 1.95 (s, 3H), 1.91 (s, 3H), 1.88 (s, 3H); purity by HPLC = 97 %; ESI MS calcd for $C_{40}H_{33}N_7Ru$ $[M]^{2+}$ 356.59; found 356.7 $[M]^{2+}$; UV/Vis (CH_3CN): λ^{max} (ε) 455 nm (11800 $mol^{-1}dm^3cm^{-1}$).

7 R_f=0.52 (0.1% KNO_3, 5%H_2O in MeCN); ^{1}H NMR (CD_3CN): δ 8.74 (d, *J* = 8.3 Hz, 1H), 8.68 (d, *J* = 8.3 Hz, 1H), 8.35 (d, *J* = 8.3 Hz, 1H), 8.27 (d, *J* = 8.7 Hz, 1H), 8.23 (d, *J* = 8.3 Hz, 1H), 8.13–8.20 (m, 3H), 7.94–7.98 (m, 2H), 7.86 (d, *J* = 8.3 Hz, 1H), 7.78 (d, *J* = 8.4 Hz, 1H), 7.66 (d, *J* = 8.5 Hz, 1H), 7.40–7.46 (m, 3H), 7.16 (ddd, *J* = 8.0, 5.8, 1.5 Hz 1H), 7.00–7.04 (m, 2H), 5.12 (d, *J* = 8.3 Hz, 1H), 2.11 (s, 3H), 2.00 (s, 3H), 1.98 (s, 3H), 1.90 (s, 3H); purity by HPLC = 98 %; ESI MS calcd for $C_{40}H_{32}N_6ORu$ $[M^{2+}•PF_6^-]^+$ 859.13,

$[M]^{2+}$ 357.09; found 859.3 $[M^{2+}•PF_6^-]^+$, 356.9 $[M]^{2+}$; UV/Vis (CH_3CN): λ^{max} (ε) 445 nm (7700 $mol^{-1}dm^3cm^{-1}$).

8 R_f=0.51 (0.1% KNO_3, 5%H_2O in MeCN);^{1}H NMR (CD_3CN): δ 8.72 (d, *J* = 8.3 Hz, 1H), 8.67 (d, *J* = 8.3 Hz, 1H), 8.41 (d, *J* = 8.3 Hz, 1H), 8.28 (d, *J* = 8.8 Hz, 1H), 8.23 (d, *J* = 8.4 Hz, 1H), 8.16–8.20 (m, 2H), 8.08 (d, *J* = 8.8 Hz, 1H), 7.91–7.95 (m, 2H), 7.89 (d, *J* = 8.4 Hz, 1H), 7.84 (d, *J* = 8.7 Hz, 1H), 7.73 (d, *J* = 8.4 Hz, 1H), 7.49 (d, *J* = 8.3 Hz, 1H), 7.40 (d, *J* = 8.4 Hz, 1H), 7.34 (ddd, *J* = 8.8, 7.4, 1.0 Hz, 1H), 7.09–7.14 (m, 2H), 6.92 (ddd, *J* = 8.8, 7.1, 1.2 Hz, 1H), 5.37 (d, *J* = 8.6 Hz, 1H), 2.10 (s, 3H), 2.01 (s, 3H), 1.85 (s, 3H), 1.84 (s, 3H); purity by HPLC = 99 %; ESI MS calcd for $C_{40}H_{32}N_6RuS$ $[M^{2+}•PF_6^-]^+$ 875.11, $[M]^{2+}$ 365.08; found 875.3 $[M^{2+}•PF_6^-]^+$, 365.1 $[M]^{2+}$; UV/Vis (CH_3CN): λ^{max} (ε) 445 nm (8900 $mol^{-1}dm^3cm^{-1}$).

General Preparation of $Ru(bpy)_2L$ Complexes

$Ru(bpy)_2Cl_2•2H_2O$ (120 mg, 0.23 mmol) and 2-(2-pyridyl)benzazole (0.27 mmol) were added to 6 mL of 50:50 EtOH:H_2O in a 15 mL pressure tube. The mixture was heated at 90 °C for 2 h, after which the orange solution was allowed to cool to room temperature. Addition of a saturated aq KPF_6 solution resulted in precipitation of the complex, which was extracted into methylene chloride. Purification of the orange solid was carried out by flash chromatography (silica gel, loaded in 0.1% KNO_3, 5% H_2O in MeCN). The pure complex eluted at 0.2% KNO_3, 10% H_2O in MeCN, and the product fractions were concentrated under reduced pressure. A saturated aq solution of KPF_6 was added, and the complex was extracted into CH_2Cl_2, followed by removal of the solvent under reduced pressure to give an orange solid.

9 R_f=0.60 (0.1% KNO_3, 5%H_2O in MeCN);^{1}H NMR (CD_3CN): δ 8.40–8.44 (m, 3H), 8.30 (d, *J* = 8.2 Hz, 1H), 7.92–8.01 (m, 5H), 7.88 (td, *J* = 8.0, 1.5 Hz, 1H), 7.75–7.90 (m, 2H), 7.69 (ddd, *J* = 8.2, 7.5, 1.6 Hz, 1H), 7.55 (ddd, *J* = 6.0, 1.6, 0.8 Hz, 1H), 7.46 (dt, *J* = 8.0, 1.0 Hz, 1H), 7.31–7.35 (m, 3H), 7.19–7.27 (m, 3H), 6.89 (ddd, *J* = 8.0, 5.8, 1.6 Hz, 1H), 6.68 (ddd, *J* = 8.0, 6.8, 0.8 Hz, 1H), 6.47 (ddd, *J* = 8.8, 6.8, 1.2 Hz, 1H), 5.38 (d, *J* = 7.5 Hz, 1H); purity by HPLC = 98 %; ESI MS calcd for $C_{33}H_{25}N_6Ru$ $[M]^+$ 607.12; found 607.1 $[M]^+$; UV/Vis (CH_3CN): λ^{max} (ε) 480 nm (8600 $mol^{-1}dm^3cm^{-1}$).

10 R_f=0.38 (0.1% KNO_3, 5%H_2O in MeCN);^{1}H NMR (CD_3CN): δ 8.51–8.54 (m, 3H), 8.47 (d, *J* = 8.1 Hz, 1H), 8.44 (d, *J* = 8.1 Hz, 1H), 7.96–8.15 (m, 6H), 7.80–7.87 (m, 3H), 7.71–7.75 (m, 2H), 7.47 (ddd, *J* = 8.0, 5.6, 1.3 Hz, 1H), 7.37–7.44 (m, 4H), 7.34 (ddd, *J* = 8.0, 5.6, 1.2 Hz, 1H), 7.05 (ddd, *J* = 8.8, 7.4, 1.1 Hz, 1H), 5.82 (d, *J* = 8.3 Hz, 1H); purity by HPLC = 99 %; ESI MS calcd for $C_{32}H_{25}N_7Ru$ $[M]^{2+}$ 304.56; found 304.6 $[M]^{2+}$; UV/Vis (CH_3CN): λ^{max} (ε) 455 nm (13100 $mol^{-1}dm^3cm^{-1}$).

11 R_f=0.45 (0.1% KNO_3, 5%H_2O in MeCN);^{1}H NMR (CD_3CN): δ 8.51–8.54 (m, 3H), 8.48 (d, *J* = 7.9 Hz, 1H), 8.45 (d, *J* = 8.2 Hz, 1H), 8.01–8.19 (m, 6H), 7.94 (d, *J* = 5.4 Hz, 1H), 7.88 (d, *J* = 8.5 Hz, 1H), 7.77–7.82 (m, 3H), 7.61 (ddd, *J* = 8.8, 7.5, 1.1 Hz, 1H), 7.55 (ddd, *J* = 8.0, 5.6, 1.3 Hz, 1H), 7.42–7.49 (m, 3H), 7.39 (ddd, *J* = 8.0, 5.6, 1.2 Hz, 1H), 7.28 (ddd, *J* = 8.8, 7.6, 0.9 Hz, 1H), 5.96 (d, *J* = 8.2 Hz, 1H); purity by HPLC = 95 %; ESI MS calcd for

$C_{32}H_{25}N_6ORu$ $[M]^{2+}$ 305.06; found 305.1 $[M]^{2+}$; UV/Vis (CH_3CN): λ^{max} (ε) 450 nm (12600 $mol^{-1}dm^3cm^{-1}$).

12 R_f=0.45 (0.1% KNO_3, 5%H_2O in MeCN);^{1}H NMR (CD_3CN): δ 8.51–8.54 (m, 4H), 8.44 (d, *J* = 8.1 Hz, 1H), 8.20 (d, *J* = 8.1 Hz, 1H), 8.04–8.16 (m, 4H), 8.01 (td, *J* = 8.0, 1.4 Hz, 1H), 7.92 (d, *J* = 5.8 Hz, 1H), 7.84 (d, *J* = 5.2 Hz, 1H), 7.74 (d, *J* = 5.7 Hz, 1H), 7.69 (d, *J* = 5.5 Hz, 1H), 7.67 (d, *J* = 5.3 Hz, 1H), 7.57 (ddd, *J* = 8.4, 7.2, 1.0 Hz, 1H), 7.45–7.49 (m, 2H), 7.37–7.42 (m, 2H), 7.35 (ddd, *J* = 8.0, 5.6, 1.2 Hz, 1H), 7.27 (ddd, *J* = 8.8, 7.3, 1.1 Hz, 1H), 6.31 (d, *J* = 8.5 Hz, 1H); purity by HPLC = 98 %; ESI MS calcd for $C_{32}H_{24}N_6RuS$ $[M^{2+}•PF_6^-]^+$ 771.05, $[M]^{2+}$ 313.04; found 771.2 $[M^{2+}•PF_6^-]^+$, 313.1 $[M]^{2+}$; UV/Vis (CH_3CN): λ^{max} (ε) 445 nm (13100 $mol^{-1}dm^3cm^{-1}$).

Counter ion exchange

Compounds **5**–**12** were converted to Cl^- salts by dissolving 5–20 mg of product in 1–2 mL methanol. The dissolved product was loaded onto an Amberlite IRA-410 chloride ion exchange column, eluted with methanol, and the solvent was removed in vacuo.

Cytotoxicity Assay

HL60 cells were plated at 30,000 cell per well in Opti-MEM media with 1% FBS and pen-strep in 96 well plates. Compounds were serially diluted in opti-MEM with 1% FBS and pen-strep in a 96 well plate and then added to the cells. They were then irradiated with 29.1 J/cm^2 light (>450 nm using the Indigo LED) for 1 minute or kept in the dark. The cells were incubated with the compounds for 72 h followed by the addition of resazurin. The plates were incubated for 3 h and then read on a SpectraFluor Plus plate reader with an excitation filter of 535 nm and emission of 595 nm.

DNA Gel Electrophoresis

Compounds were mixed with 40 μg/mL pUC19 plasmid DNA in 10 mM potassium phosphate buffer, pH 7.4. To determine the effect of light, samples were irradiated with a 470 nm LED for a total light dose of 46.8 J/cm^2. Samples were then incubated for 12 h at room temperature in the dark. Single- and double-strand DNA break controls were prepared, and the DNA samples were resolved on agarose gels, as described previously.[8a] In brief, samples were resolved on a 1% agarose gels prepared in tris-acetate buffer with 0.3 μg of plasmid/lane. The gels were stained with 0.5 μg/mL ethidium bromide in tris-acetate buffer at room temperature for 40 min, destained with tris-acetate buffer, and imaged on a ChemiDoc MP System (Bio-Rad).

Singlet Oxygen Assay

Compounds were serially diluted in 10 mM potassium phosphate buffer, pH 7.4, with ~5μM Singlet Oxygen Sensor Green reagent in 96 well plates. The plates were read on a SpectraFluor Plus plate reader with an excitation filter of 485 nm and emission of 535 nm in a dark and after 1h irradiation with a 470 nm LED for total light dose of 46.8 J/cm^2.

Cell Cycle Analysis

HL60 cells were plated in opti-MEM with 1% FBS at a density of 500,000 cells/ml in 6-well plates. The compounds were added and incubated with the cells from 0 to 12 h. For each time point the cells were transferred to FACS tubes, pelleted, washed with PBS, followed by the addition of cold 70% ethanol and incubated on ice for one hour to fix the cells. Cells were then centrifuged at 2000 rpm for 5 minutes, and resuspended in 1 ml PBS for each tube. The tubes were centrifuged at 2000 rpm for 5 minutes, the supernatant was aspirated and the cells were resuspended in 0.5 mL PI staining buffer (20 mg/mL PI in PBS, 0.2 mg/mL RNAse, 0.1% TritonX-100) and incubated at room temperature for 30 minutes. Samples were run through the flow cytometer and data was analyzed with ModFit and FlowJo.

Crystallography

Single crystals of compounds **6–8** were grown from methylene chloride or acetone by vapor diffusion of diethyl ether. They were mounted in inert oil and transferred to the cold gas stream of the diffractometer. X-ray diffraction data were collected at 90.0(2) K on either a Nonius kappaCCD diffractometer using Mo$K\alpha$ X-rays or on a Bruker-Nonius X8 Proteum diffractometer with graded-multilayer focused Cu$K\alpha$ X-rays. Raw data were integrated, scaled, merged and corrected for Lorentz-polarization effects using either the HKL-SMN package[19] or the APEX2 package.[20] Corrections for absorption were applied using SADABS[21] and XABS2.[22] The structures were solved by SHELXT,[23] and refined against F^2 by weighted full-matrix least-squares using SHELXL-2014.[24] For compound **8** the SQUEEZE routine[25] was used to treat disordered solvent. Hydrogen atoms were placed at calculated positions and refined using a riding model. Non-hydrogen atoms were refined with anisotropic displacement parameters. Structures were checked using check CIF tools in Platon[26] and by an R-tensor.[27] Crystal data and relevant details of the structure determinations are summarized below and selected geometrical parameters are given in Table 1.

Crystal data (6)—$C_{41}H_{35}Cl_2F_{12}N_7P_2Ru$, Mr = 1087.67, Monoclinic, $P2_1/c$, a = 12.3286(2) Å, b = 18.7316(3)Å, c = 18.1692(3) Å, β = 94.943(1)°, V = 4180.29(12)Å^3, Z = 4, ρ = 1.728 mg m^{-3}, μ = 5.802 mm^{-1}, F(000) = 2184, crystal size = 0.300×0.120×0.060 mm, θ(max) = 68.373°, 56392 reflections collected, 7596 unique reflections (R_{int} = 0.0433), GOF = 1.065, R_1 = 0.0408 and wR_2 = 0.0933 [I > 2σ(I)], R_1 = 0.0436 and wR_2 = 0.0949 (all indices), largest difference peak/hole = 1.531/−1.465 eÅ^{-3}.

Crystal data (7)—$C_{48.29}H_{50.15}F_{12}N_6O_{3.50}P_2Ru$, Mr = 1161.55, Monoclinic, C2/c, a = 23.0734(5) Å, b = 19.9646(5) Å, c = 22.6098(5) Å, β = 108.547(1)°, V = 9874.3(4) Å^3, Z = 8, ρ = 1.563 mg m^{-3}, μ = 4.028 mm^{-1}, F(000) = 4735, crystal size = 0.230×0.180×0.030 mm, θ(max) = 68.355°, 60921 reflections collected, 8945 unique reflections (R_{int} = 0.0643), GOF = 1.036, R_1 = 0.0409 and wR_2 = 0.0985 [I > 2σ(I)], R_1 = 0.0561 and wR_2 = 0.1067 (all indices), largest difference peak/hole = 0.631/−0.544 eÅ^{-3}.

Crystal data (8)—$C_{89}H_{82}F_{24}N_{12}O_3P_4Ru_2S_2$, Mr = 2213.80, Triclinic, P-1, a = 14.2840(2) Å, b = 17.5165(2)Å, c = 20.0585(3)Å, α = 91.5547(8)°, β = 90.7709(8)°, γ =

110.9785(7)°, V = 4682.91(11)Å^3, Z = 2, ρ = 1.570 mg m^{-3}, μ = 0.539 mm^{-1}, F(000) = 2240, crystal size = 0.320×0.280×0.270 mm, θ(max) = 27.509°, 136315 reflections collected, 21482 unique reflections (R_{int} = 0.0402), GOF = 1.054, R_1 = 0.0445 and wR_2 = 0.1153 [I > 2σ(I)], R_1 = 0.0688 and wR_2 = 0.1297 (all indices), largest difference peak/hole = 1.247/−0.749 eÅ^{-3}.

Supplementary Material

Refer to Web version on PubMed Central for supplementary material.

Acknowledgments

This work was supported by the National Institutes of Health (5R01GM107586). The X8 Proteum was funded by the NSF (MRI CHE-0319176). Mass spectroscopy analysis was performed at the University of Kentucky Environmental Research Training Laboratory (ERTL).

References

1. Siegel RL, Miller KD, Jemal A. CA Cancer J Clin. 2016; 66:7–30. [PubMed: 26742998]
2. Galanski M, Jakupec MA, Keppler BK. Curr Med Chem. 2005; 12:2075–2094. [PubMed: 16101495]
3. a) Hannon MJ. Pure and Applied Chemistry. 2007; 79:2243–2261.b) Griffin AM, Butow PN, Coates AS, Childs AM, Ellis PM, Dunn SM, Tattersall MH. Ann Oncol. 1996; 7:189–195. [PubMed: 8777177]
4. a) Antonarakis ES, Emadi A. Cancer Chemother Pharmacol. 2010; 66:1–9. [PubMed: 20213076] b) Barry NP, Sadler PJ. Chem Commun (Camb). 2013; 49:5106–5131. [PubMed: 23636600]
5. Bergamo A, Gaiddon C, Schellens JH, Beijnen JH, Sava G. J Inorg Biochem. 2012; 106:90–99. [PubMed: 22112845]
6. Ang WH, Casini A, Sava G, Dyson PJ. Journal of Organometallic Chemistry. 2011; 696:989–998.
7. Glazer EC. Israel Journal of Chemistry. 2013; 53:391–400.
8. a) Howerton BS, Heidary DK, Glazer EC. J Am Chem Soc. 2012; 134:8324–8327. [PubMed: 22553960] b) Wachter E, Heidary DK, Howerton BS, Parkin S, Glazer EC. Chem Commun. 2012; 48:9649–9651.c) Hidayatullah AN, Wachter E, Heidary DK, Parkin S, Glazer EC. Inorg Chem. 2014; 53:10030–10032. [PubMed: 25198057]
9. Heidary DK, Glazer EC. Chembiochem. 2014; 15:507–511. [PubMed: 24482049]
10. a) Farrer NJ, Salassa L, Sadler PJ. Dalton Trans. 2009:10690–10701. [PubMed: 20023896] b) Mari C, Pierroz V, Ferrari S, Gasser G. Chemical Science. 2016; 6:2660–2668.
11. a) N M-A, Busto M, Leal JM, Rodríguez AM, Domínguez F, Acuña MI, Espino G, García B. Organometallics. 2015; 34:319–327.b) Martinez-Alonso M, Busto N, Jalon FA, Manzano BR, Leal JM, Rodriguez AM, Garcia B, Espino G. Inorg Chem. 2014; 53:11274–11288. [PubMed: 25302401]
12. Ong JX, Yap CW, Ang WH. Inorg Chem. 2012; 51:12483–12492. [PubMed: 23121648]
13. Yellol GS, Donaire A, Yellol JG, Vasylyeva V, Janiak C, Ruiz J. Chem Commun (Camb). 2013; 49:11533–11535. [PubMed: 24177492]
14. a) Wu F, Chamchoumis CM, Thummel RP. Inorg Chem. 2000; 39:584–590. [PubMed: 11229581] b) Richardson CMFC, Keene FR, Steel PJ. Australian Journal of Chemistry. 2008; 61:183–188.c) Yi H, Crayston JA, Irvine JTS. Dalton Trans. 2003:685–691.
15. Shen WZ, Trotscher-Kaus G, Lippert B, Trans Dalton. 2009:8203–8214.
16. Liu YJ, Chao H, Yu HJ, Yuan YX, Ji LN. ActaCrystallogr Sect E: Struct REp Online. 2006; 62:m585.
17. Unfortunately, attempts to quantify the singlet oxygen using 1,3-diphenylisobenzofuran (DPBF) failed due to poor stability of the reagent under irradiation. The procedure used was reported

byZhang W, Li B, Ma H, et al. ACS Appl Mater Interfaces. 2016; 8(33):21465–71. [PubMed: 27483010]

18. a) Cravotto G, Demartin F, Palmisano G, Penoni A, Radice T, Tollari S. J Organomet Chem. 2005; 690:2017–2026.b) Sedachat N, Naimi-Jamal MR, Mokhtari J. Current Chemistry Letters. 2014; 3:57–62.
19. O, Z., Minor, W. Processing of x-ray diffraction data collected in oscillation mode. Carter, JRMSCW., editor. Vol. 276. Academic Press; 1997.
20. APEX2. Programs for data collection and data reduction. Bruker-Nonius; Madison WI. USA: 2012.
21. Krause L, Herbst-Irmer R, Sheldrick GM, Stalke D. J Appl Cryst. 2015; 48:3–10. [PubMed: 26089746]
22. Parkin S, Moezzi B, Hope H. J Appl Cryst. 1995; 28:53–56.
23. Sheldrick GM. Acta Cryst. 2015; A71:3–8.
24. Sheldrick GM. Acta Cryst. 2015; C71
25. van der Sluis P, Spek AL. Acta Cryst. 1990; A46:194–201.
26. Spek AL. Acta Cyst. 2009; D65:148–155.
27. Parkin S. Acta Cyst. 2000; A56:157–162.

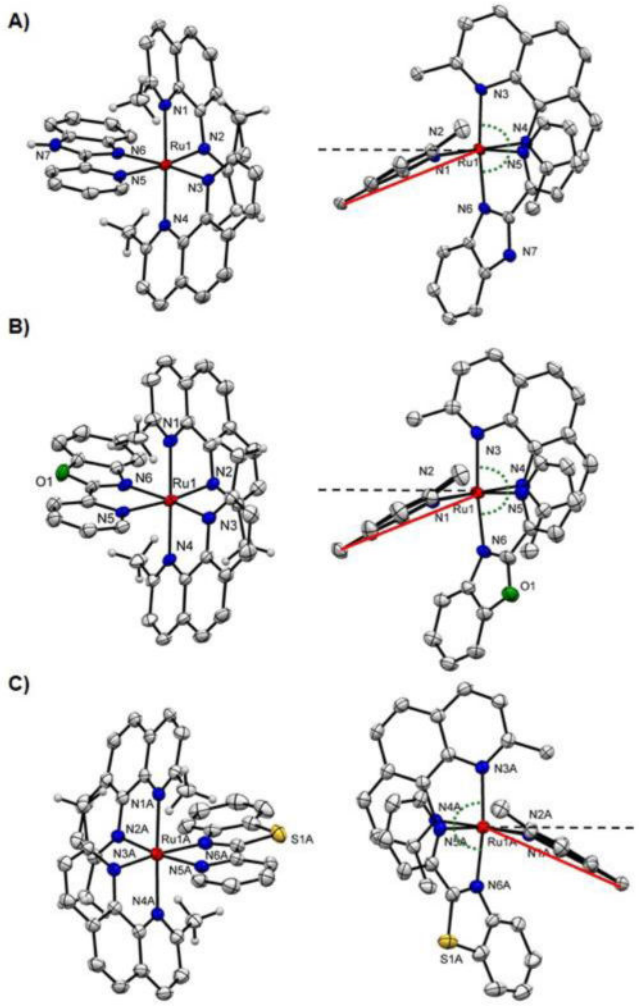

Figure 1.

Ellipsoid plot of ruthenium complexes A) (Δ)-**6**, B) (Δ)-**7**, C) (Λ)-**8** at 50% probability with H atoms omitted for clarity. Right column: side views highlighting the distortion of the dmphen ligand. The black dashed lined indicates the normal plane and the angle between red and black dash line represents the ligand bend. Note: for **8** only one cation of the asymmetric unit is shown.

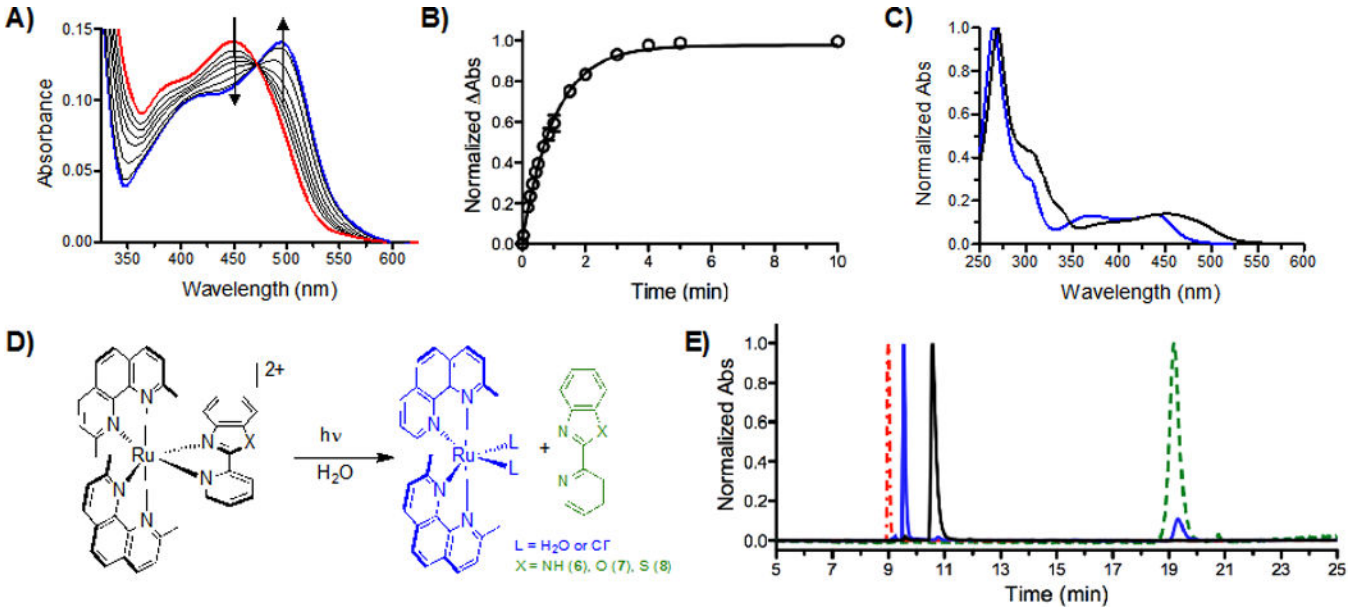

Figure 2.

A) Photoejection of **7** (30 μM) in water for 0–240 min irradiation followed by UV/Vis absorption; red = initial, blue = final. B) The photoejection kinetics for **7**; reaction was complete in less than 5 min. Determination of photoejection products by HPLC: C) Absorption profile of **7** (black, retention time = 10.56 min) and the photochemical product (blue, retention time = 9.55 min); note that the presence of CH_3CN changes the absorption profile; see Figure S28). D) Photoejection reaction scheme for **6**–**8**, showing the photochemical products. E) HPLC chromatogram of **7** before (black) and after irradiation for 1 min with the Indigo LED (blue), in comparison with started ligands: dmphen (red) and pbo (green). The same light dose was used in the cell studies.

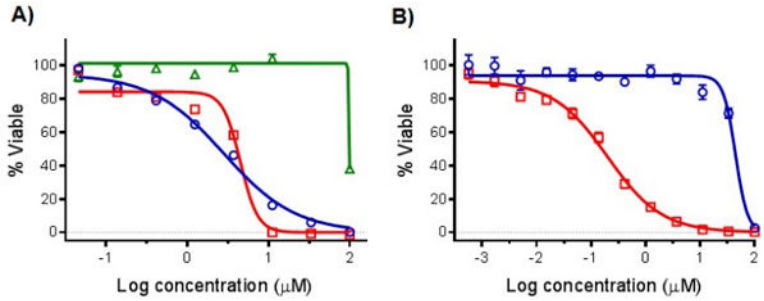

Figure 3.

Cytotoxicity dose responses of ruthenium complexes and parent ligand on HL60 cells: A) **2** and **6**; B) **10**. Dark conditions (circles, blue line); irradiated samples, 1 min >450 nm light using the Indigo LED (29.1 J/cm^2; squares, red line); ligand **2** (triangles, green line). (n = 3).

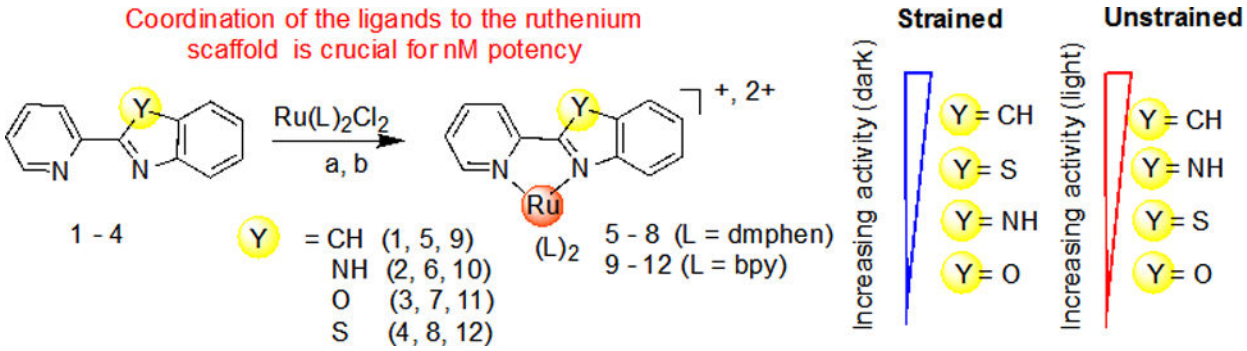

Figure 4.

SAR Analysis for Antitumor Ru(II) Complexes with 2-(2-Pyridyl)Benzazole Ligands

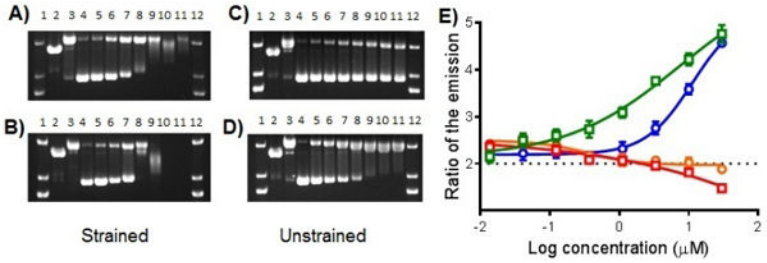

Figure 5.

Agarose gel electrophoresis of 40 μg/mL pUC19 plasmid (10 mM phosphate buffer, pH 7.5) with light-activated Ru(II) compounds. Dose response profiles: (A) **6**; (B) **8**; (C) **10**; (D) **12**; Lanes 1 and 12, DNA molecular weight standard; lane 2, linear pUC19; lane 3, relaxed circle ($Cu(phen)_2$ reaction with pUC19); lanes 4−11, 0, 7.8, 15.6, 31.25, 62.5, 125, 250, and 500 μM compound. E) Singlet oxygen generation dose responses of ruthenium complexes: **6** (circles, orange line); **8** (squares, red line); **10** (circles, blue line); and **12** (squares, green line). (n = 2). The data is shown as a ratio of the emission of the sensor after irradiation with the compound vs. without irradiation. The slight downward curve for **8** suggests this compound quenches singlet oxygen at high doses.

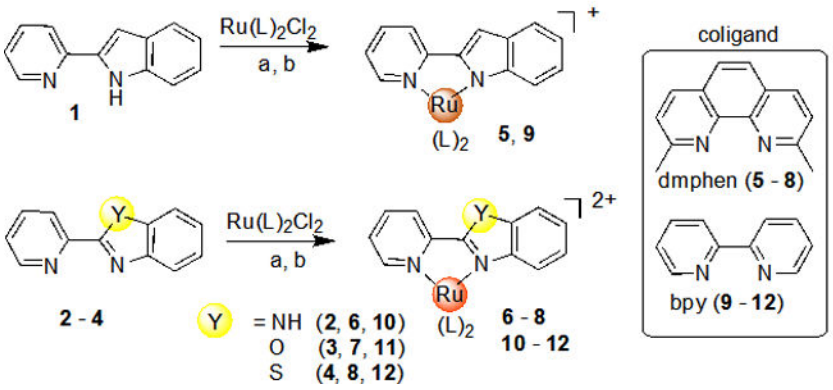

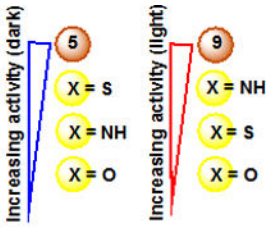

Scheme 1.

Synthesis of Ru(II) complexes with bioisosteric 2-(2-pyridyl)benzazole ligands. Reagents, conditions and yields: (a) $Ru(dmphen)_2Cl_2$ (1.0 eq), ethylene glycol, 100–120 °C for 2 h (**5–8**), 20–30%; (b) $Ru(bpy)_2Cl_2$ (1.0 eq), ethanol-water (1:1), 90 °C for 2 h (**9–12**), 45–95%.

Table 1

Selected bond lengths (Å), bond angles (°) and torsion angles (°) of **6**–**8**.

	6	7	8
Bond Lengths (Å)			
Ru-N1	2.114(3)	2.114(3)	2.114(2)
Ru-N2	2.097(3)	2.103(3)	2.102(2)
Ru-N3	2.100(3)	2.090(3)	2.097(2)
Ru-N4	2.120(3)	2.105(3)	2.108(2)
Ru-N5	2.109(3)	2.106(3)	2.097(2)
Ru-N6	2.099(3)	2.112(3)	2.112(2)
Bond Angles (°)			
N1-Ru-N2	79.45(11)	79.73(10)	79.06(9)
N1-Ru-N3	100.6(1)	100.96(11)	101.40(9)
N1-Ru-N4	178.35(11)	178.86(11)	177.52(9)
N1-Ru-N5	95.9(1)	95.99(10)	96.07(9)
N1-Ru-N6	81.86(10)	80.24(11)	82.05(9)
N2-Ru-N3	94.57(10)	94.56(10)	93.35(9)
N2-Ru-N4	102.1(1)	100.78(10)	103.19(9)
N2-Ru-N5	170.3(1)	171.59(10)	171.30(9)
N2-Ru-N6	92.78(10)	94.05(10)	94.03(9)
N3-Ru-N4	79.88(11)	80.04(11)	79.62(9)
N3-Ru-N5	94.66(10)	93.36(10)	94.69(9)
N3-Ru-N6	172.56(10)	171.39(10)	172.34(9)
N4-Ru-N5	82.49(10)	83.38(10)	81.57(9)
N4-Ru-N6	97.46(10)	98.69(10)	96.67(9)
N5-Ru-N6	78.06(10)	78.02(10)	78.07(10)
Torsion Angles (°)			
N1-C6-C7-N2	2.1(4)	1.2(5)	−2.2(4)
Ru-N1-C2-C3	−167.4(3)	−167.1(3)	163.2(2)
Ru-N2-C11-C10	164.0(2)	165.9(3)	−162.8(2)
N3-C20-C21-N4	1.8(5)	2.0(4)	−4.0(4)
Ru-N3-C16-C17	169.4(3)	168.7(3)	−171.0(2)
Ru-N4-C25-C24	−165.6(2)	−167.8(2)	162.3(2)
N5-C33-C34-N6	1.8(4)	3.0(5)	−2.3(4)
Ru-N5-C29-C30	176.0(3)	175.3(3)	−177.4(2)
L1 bend [a]	22.6	22.6	22.7
L2 bend [b]	21.4	19.5	21.6

[a] L1 bend = average angle (N3-Ru-C13/C14) – 90°; L1 – dmphen where L is N1 and N2

[b] L2 bend = average angle (N2-Ru-C27/C28) – 90°; L2 – dmphen where L is N3 and N4

Table 2

Photophysical and photochemical properties for **5**–**12** for various reaction conditions.

Compound	λ_{max} (nm)		$t_{1/2}$ (min)	
	water	Opti-MEM	water	Opti-MEM
5	475	475	47.3±2.80	n.r.*
6	455	455	1.17±0.08	10.38±0.33
7	450	450	1.03±0.09	1.42±0.04
8	440	440	0.34±0.04	0.66±0.002
9	490	490	66.02±13.11	66.11±5.95
10	455	435	n.r.	n.r.
11	450	450	n.r.	n.r.
12	445	450	n.r.	n.r.

* n.r. = no reaction

Table 3

Cytotoxicity IC_{50} Values for 2-(2-Pyridyl)Benzazole Ligands and Ru Complexes in the HL60 Cancer Cell Line

Comp.	Coligand	Y	Dark IC_{50} [μM]	Light[a] IC_{50} [μM]	PI
1	–	CH	>100	n.d.[b]	n.d.
2	–	NH	>100	n.d.	n.d.
3	–	O	>100	n.d.	n.d.
4	–	S	>100	n.d.	n.d.
5	dmphen	CH	0.34 (±0.008)	0.034 (±0.001)	10
6	dmphen	NH	2.79 (±0.31)	4.49 (±0.07)	0.6[c]
7	dmphen	O	4.54 (±1.37)	3.43 (±0.75)	1.3
8	dmphen	S	1.55 (±0.41)	4.55 (±1.73)	0.3[c]
9	bpy	CH	1.24 (±0.008)	0.18 (±0.001)	7.3
10	bpy	NH	44.8 (±0.4)	0.20 (±0.017)	224
11	bpy	O	63.5 (±8.3)	5.18 (±0.047)	12.2
12	bpy	S	83.3 (±1.2)	0.94 (±0.09)	88
Cisplatin	–	–	3.1 (±0.2)	3.1 (±0.2)	1

[a] Using the Loctite Indigo LED array (light dose of 29.1 J/cm^2)

[b] n.d. – not determined.

[c] The PI values reflect differences in the slopes of the dose response curves, and likely indicate that different cytotoxicity mechanisms are responsible for cell death in the dark vs. light conditions.